

Is Mycobacterial InhA a Suitable Target for Rational Drug Design?

Julien Rizet, Laurent Maveyraud, David Rengel, Valérie Guillet, Gabriel Publicola, Frédéric Rodriguez, Christian Lherbet,* and Lionel Mourey*

InhA, an NAD-dependent enoyl-acyl carrier protein reductase, is involved in the biosynthesis of mycolic acids, specific lipids to mycobacteria. InhA is the target of isoniazid, a first-line antituberculosis drug used since the 1950s. Isoniazid is a prodrug that needs to be activated by the catalase-peroxidase KatG. Due to resistance problems, a substantial amount of work has been carried out to identify or design direct inhibitors of InhA, demonstrating that this enzyme is still considered a relevant target for the discovery of new antituberculosis drugs. Much of this work included the resolution of crystallographic structures. Indeed, over a hundred structures have been deposited in the Protein

Data Bank for different forms of the enzyme (apo, holo, and complexes), demonstrating a real crystalline polymorphism. Taken together, these structures constitute a valuable dataset. However, the complete decoding of the enzyme's properties and its inhibition literally comes up against its molecular plasticity at the level of a motif essential to the definition of the active site: the substrate-binding loop. In this article, a detailed analysis of this structural dataset is proposed, describing in particular the different families of inhibitors and attempting to establish structural links of causality.

1. Introduction

The enoyl-acyl carrier protein (ACP) reductase InhA is the main target of isoniazid (isonicotinic acid hydrazide, INH), a first-line drug used to treat tuberculosis (TB) caused by the pathogen *Mycobacterium tuberculosis* (MTB). First introduced in 1952, INH—"an inexpensive, well-tolerated, and safe molecule"—was considered a major breakthrough to combat the disease.^[1] More than 70 years later, INH remains a major component for the treatment of drug-susceptible TB, in combination with three other first-line TB medicines (i.e., rifampicin, pyrazinamide, and ethambutol).^[2]


An impressive amount of biological, biochemical, and structural information have been published since 1994, when InhA was formally identified as the target of INH and its structural analogue ethionamide (ETH).^[3] Previously, it had been shown to inhibit the biosynthesis of mycolic acids, long-chain α -alkylated β -hydroxylated fatty acids, the major lipids in the MTB envelope.^[4]


Further biochemistry work revealed that InhA catalyzes the NADH-dependent reduction of *trans*-2-enoyl-ACP substrates as part of the type II fatty acid synthesis (FAS-II) system required for mycolic acid biosynthesis (Scheme 1).^[5] This was corroborated by the first crystal structure of the enzyme in complex with NADH.^[6] In fact, INH is a prodrug that requires activation by the catalase-peroxidase KatG to generate the isonicotinoyl-NADH (INH-NADH) adduct that inhibits InhA (Scheme 1). Although long debated, the chemical nature of this adduct, its mechanism of formation, and the corresponding molecular mechanism of inhibition have been clarified thanks to several crystal structures of the InhA·INH-NADH complex (see^[7] and references therein).

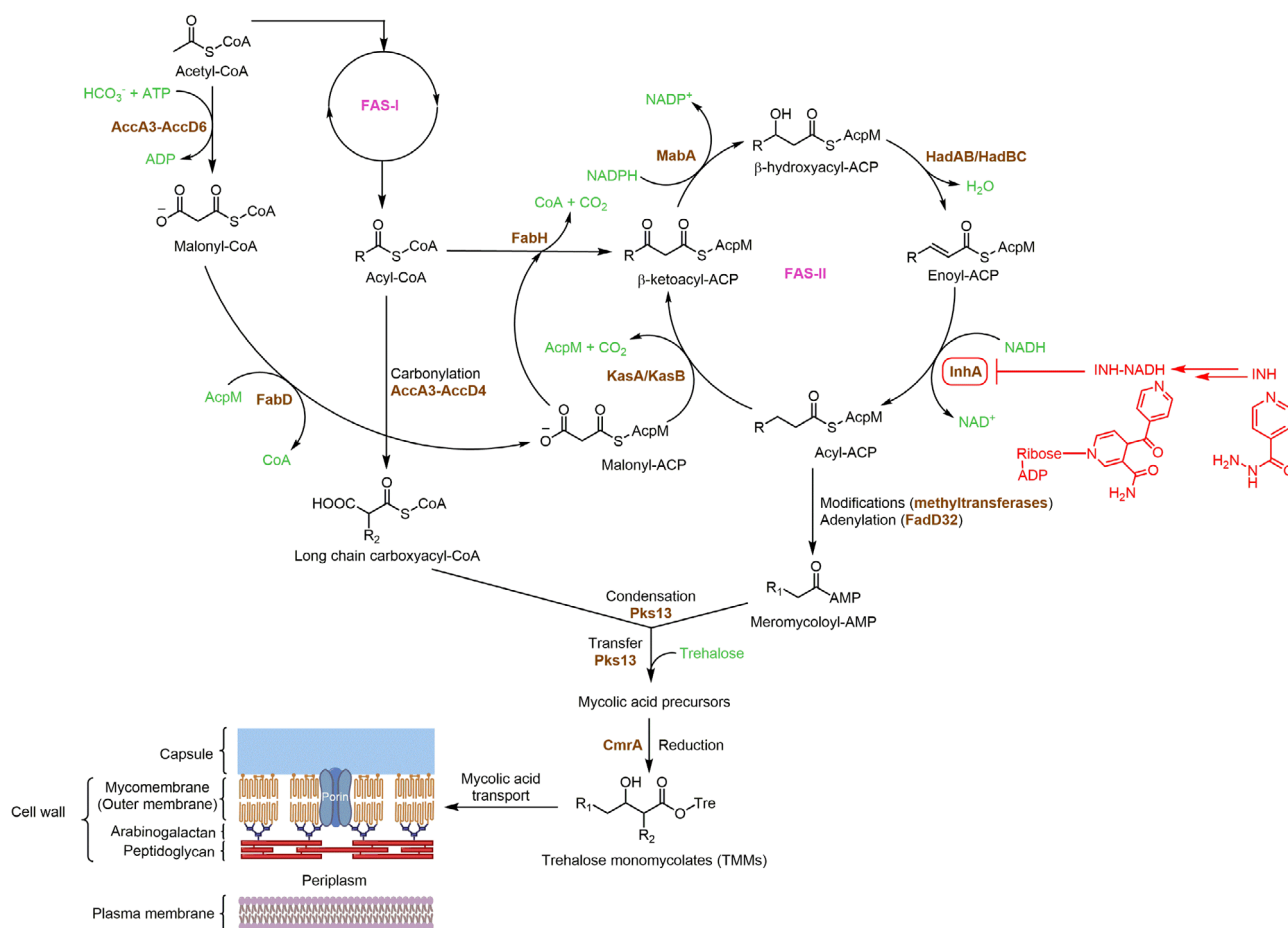
Unfortunately, bacterial resistance to INH was identified as early as the first clinical trials. Resistance to INH is mainly due to missense mutations in the *katG* gene and to a lesser extent in the promoter region of *inhA* or in its coding region.^[8] Overall, INH-resistant and rifampicin-susceptible TB is the most widespread form of drug resistance in the world (besides resistance to streptomycin), and it is associated with a higher risk of acquiring greater drug resistance.^[2] Thus, multidrug-resistant TB (MDR-TB), due to resistance to INH and rifampicin, and rifampin-resistant TB (RR-TB) are of particular concern. In 2023, 1.25 million people died from TB, 10.8 million people developed the disease, and 400 000 people developed MDR- or RR-TB.^[9] Hence, TB still represents a burden and a threat despite the recent approval of new second-line drugs (bedaquiline, delamanid, and pretomanid), for which resistance is already emerging,^[10] making the development of new medicines crucial. From this point of view, given the unique and essential nature of the mycobacterial cell envelope for the viability and pathogenicity of mycobacteria, inhibition of the biosynthesis pathway of its major lipidic constituents (i.e., mycolic acids), in particular the specific FAS-II system,

J. Rizet, L. Maveyraud, D. Rengel, V. Guillet, G. Publicola, L. Mourey
Institut de Pharmacologie et de Biologie Structurale (IPBS)
Université de Toulouse, CNRS, Université Toulouse III – Paul Sabatier (UT3)
205 route de Narbonne, BP 64182, 31077 Toulouse Cedex 4, France
E-mail: lionel.mourey@ipbs.fr

J. Rizet, F. Rodriguez, C. Lherbet
Synthèse et Physico-Chimie de Molécules d'Intérêt Biologique (SPCMIB)
Université de Toulouse, CNRS, Université Toulouse III – Paul Sabatier (UT3)
118 route de Narbonne, 31062 Toulouse Cedex 09, France
E-mail: christian.lherbet@univ-tlse3.fr

 Supporting information for this article is available on the WWW under <https://doi.org/10.1002/cmdc.202500079>

 © 2025 The Author(s). ChemMedChem published by Wiley-VCH GmbH. This is an open access article under the terms of the Creative Commons Attribution-NonCommercial-NoDerivs License, which permits use and distribution in any medium, provided the original work is properly cited, the use is non-commercial and no modifications or adaptations are made.



Scheme 1. Mycolic acid biosynthesis and inhibition of InhA by INH. Two fatty acid synthesis (FAS) systems are involved. The FAS-I system synthesizes fatty acids which, on the one hand, provide the alkylated chain of mycolic acids and, on the other, feed the FAS-II system which elongates them to form the meromycolic chain. After carboxylation for one and formation of an AMP derivative for the other, these two chains are then condensed and transferred to the carrier trehalose to generate, after reduction, trehalose monomycolates (TMMs). After transport, mycolic acids take part in the mycomembrane where they are covalently bound to arabinogalactan or trehalose. At some stage in the synthesis, chemical modifications are introduced into the meromycolic chain by methyltransferases. The names of the enzymes involved are colored brown. Inhibition of InhA through the formation of the INH-NADH adduct from INH and NADH is colored red.

remains a relevant reservoir of targets.^[11] Thus, continuous efforts have been made over the years to design and develop direct inhibitors of InhA, which would overcome isoniazid resistance. The aim of this article is to provide an update on the literature, focusing on aspects of rational drug design, and in particular on the contribution of crystallography, superseding from this point of view previous analyses of the Protein Data Bank,^[12] and outlining its strengths and pitfalls.

2. Results and Discussion

2.1. InhA is Highly Represented in the Protein Data Bank

As of January 2025, the Protein Data Bank (PDB) contained 116 InhA crystal structures: 108 for the MTB enzyme (MTB-InhA), 3 for the *M. abscessus* enzyme, 2 for the *M. fortuitum* enzyme, 2 for the *M. kansasii* enzyme, and 1 for the *M. leprae* enzyme. Table S1 (see Supporting Information) illustrates the crystal polymorphism of InhA, with different crystal systems, different space groups,

different cell parameters, and different numbers of molecules per asymmetric unit (a.u.). The corresponding crystallization conditions also involve a large number of precipitating agents (Figure S1, Supporting Information). Of the three most common crystal systems (Table S1, Supporting Information), 2-methyl-2,4-pentanediol (MPD) and low-molecular-weight polyethylene glycols (PEGs) favor the formation of hexagonal crystals, while high-molecular-weight PEGs favor monoclinic and orthorhombic forms (Figure S1, Supporting Information). The different forms in which InhA crystallizes contain from 1 (e.g., in the most encountered hexagonal system) to 2, 4, 6, or 8 molecules in the a.u. However, it is extremely important to note that the basic building block of all crystalline forms is invariably a homotetramer with dihedral (D₂) symmetry that includes three perpendicular two-fold symmetry axes. Depending on the number of molecules (hereafter also equally termed subunits or chains, depending on the context) in the a.u., the tetrameric assembly can be based on noncrystallographic (local) 2-fold symmetry axes, crystallographic 2-fold symmetry axes, or a combination of the two. The tetrameric nature of InhA found in all X-ray structures

correlates well with observations made in solution,^[7b,13] by two-hybrid experiments,^[14] and also with the tetrameric state found for the FabI family of FAS-II enoyl reductases.^[15] However, to the best of our knowledge, the existence of a tetrameric form of InhA in mycobacteria has never been proven.

The InhA structures deposited in the PDB were resolved at sufficiently high resolution (minimum = 3.4 Å, maximum = 1.4 Å, mean = 2.1 Å, median = 2.0 Å, standard deviation = 0.4 Å, $n = 116$) to validate—a priori—the use of X-ray crystallography to, at least, describe protein–inhibitor interactions and, at best, guide drug design. Indeed, as shown for MTB-InhA in Table 1, most deposited structures correspond to complexes with ligands, principally inhibitors. In what follows, we will focus on the 78 deposited structures of the wild-type MTB enzyme, which include 1 structure of the apo form,^[7a] 4 structures of the holo form with the cofactor in reduced form (NADH),^[6,7,16] and 1 structure for an enzyme–cofactor–substrate analogue complex.^[7b] It is noteworthy that no structure of the holo form with the cofactor in oxidized form (NAD⁺) has ever been deposited. In contrast, the structures of ternary enzyme–cofactor–inhibitor complexes were more frequently resolved in the presence of NAD⁺ (35 vs. 17 for NADH). In 9 cases, the redox state of the cofactor used could not be deduced from the information provided in the PDB file or the corresponding publication. Finally, 6 structures correspond to cofactor adduct inhibitors, including isoniazid (INH-NADH), and 5 structures correspond to other classes of competitive inhibitors.

It is worth mentioning that the method of preparation of the crystals used to solve all these structures can also vary. For

example, the 4 structures of the holo forms with NADH were obtained by incubation, in which case we refer to cocrystallization. The same applies to the ternary complex with a substrate analogue. Concerning the structures with an inhibitor and NAD⁺ (resp. NADH), 25 (resp. 6) of them were obtained by cocrystallization and 8 (resp. 11) by soaking of preformed crystals. In 2 cases (NAD⁺ + inhibitor), cocrystallization and soaking were both used. The majority, that is, 9, of the 11 structures with a competitive inhibitor were obtained by cocrystallization.

Due to the wealth of information provided by such a large quantity of structural data, difficulties and questions have arisen in extracting relevant information that would give a clearer picture from a mechanistic point of view and for better inhibition of the enzyme. First, the impact of the crystallization conditions—that is, the nature of the precipitating agent, the crystal preparation method, and the form of the cofactor (NADH or NAD⁺) used—has to be considered. Directly linked to this is the crystal polymorphism of InhA. In particular, when there is more than one chain in the a.u., that is, for structures belonging to systems other than hexagonal or tetragonal (Table S1, Supporting Information), these are not necessarily all occupied by a ligand (Table 1). Whether all chains are occupied or not, it seems to us that variations between chains are rarely, if ever, analyzed and described in the corresponding articles. This is even truer when considering the tetrameric form of the enzyme (structures are most often described at the protomer level) or structural plasticity, particularly of the substrate-binding loop (SBL), as described in the following paragraph.

Table 1. Overview of MTB-InhA structures available in the PDB.

Structure type ^{a)}	Wild-type enzyme ^{b)}			Mutants ^{c)}
	No. of structures	No. of chains	No. of chains occupied	
Apo	1	6	N/A	1
Holo-NADH	4	4	N/A	7
Holo-NAD ⁺	0	N/A	N/A	1
Holo-NAD?	1	1	N/A	2
Holo-NAD ⁺ + substrate analogue	1	6	4	0
Holo-NADH + inhibitors	17	55	44	11
Holo-NAD ⁺ + inhibitors	35	125	109	4
Holo-NAD? + inhibitors	8	20	20	0
Competitive inhibitors ^{d)}	11	23	14	4
Total	78	240	191	30

^{a)} Apo, apoenzyme; Holo, holoenzyme; NADH or NAD⁺, structure resolved in the presence of reduced or oxidized form of the cofactor, respectively; NAD?, reduced or oxidized form (information not provided). ^{b)} For the wild-type enzyme, the total number of chains in the corresponding structures and the number of chains occupied by the ligand (substrate analogue or inhibitor) are indicated. ^{c)} The following single mutants were used: Apo, S94A; Holo-NADH, T2A, I21V, I47T, S94A, D148G, Y158F; Holo-NAD?: T266D, T266E; Holo-NADH + inhibitors: T2A, S94A; Holo-NAD⁺ + inhibitors: V203A, I215A; Competitive inhibitors: I21V, S94A, I215A. ^{d)} Including competitive inhibitors for the cofactor or for both the cofactor and the substrate.

2.2. Digging Deep into the InhA Structures

In the InhA homo-tetramer, each subunit comprises 269 residues that adopt the classical fold found in short-chain dehydrogenases/reductases, a superfamily of enzymes found in all kingdoms.^[17] The tertiary structure consists of a seven-strand parallel β -sheet, sandwiched on either side by three helices (Figure 1A). One of the two helical faces is surmounted by two additional helices, H6 and H7, which form the SBL, the most variable region in InhA structures (Figure 1A). In particular, H6 and H7 adopt different positions relative to the active site, from closed to intermediate to open to partially or totally disordered conformations. Variations on H6 were documented in the previous review dedicated to InhA structures and published in 2018.^[12a] Here, we have reanalyzed the conformations adopted by H6 and H7 for the 240 chains making up the 78 available PDB structures of wild-type MTB-InhA. Our first analysis was carried out visually. We also used two indicators based on distance measurements between C α atoms of (i) residue Gly204 at the C-terminus of H6 and residue Gly104 and (ii) residue Ala211 at the N-terminus of H7 and residue Ala157. Residues 104 and 157 are found on two rigid loops (A and B) facing the SBL,^[18] which also contribute to the delineation of the active site (Figure 1A). Our pseudocorrelative analysis revealed that the measured distances cluster into sets that correspond to the open, closed, and intermediate conformational states visually identified for each of H6 and H7 (Figure 1B,C). Of course, this does not include chains for which

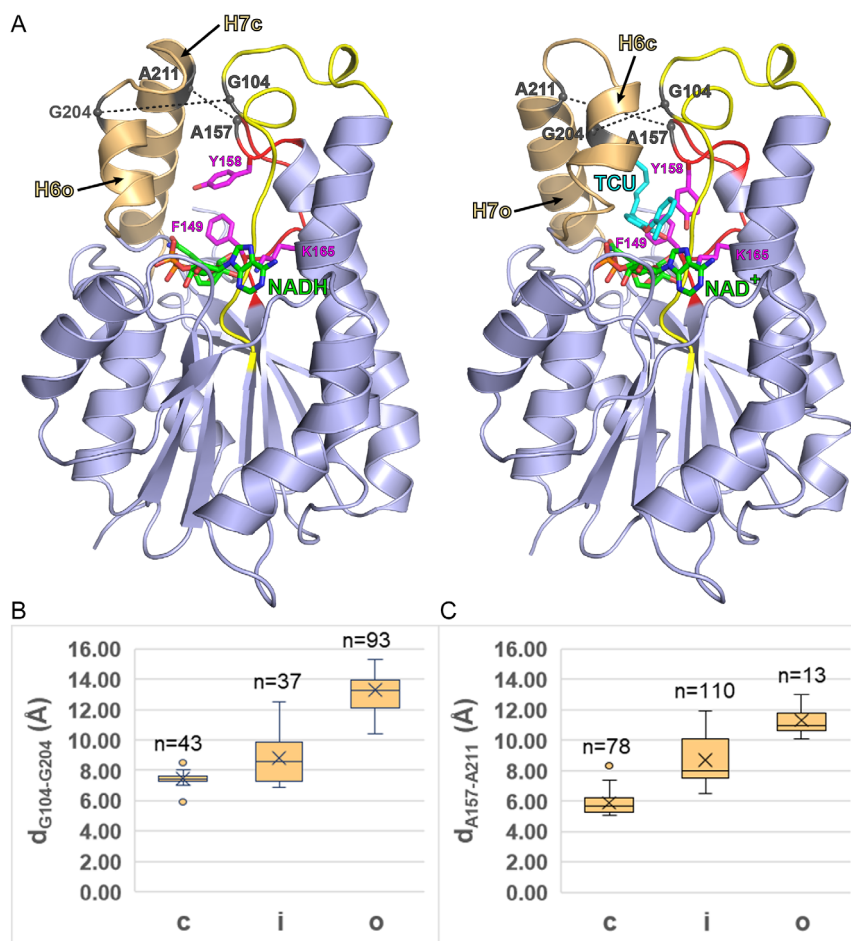


Figure 1. Wild-type MTB-InhA tertiary structure and SBL variability. A) Two examples of the different conformations of helices H6 and H7: H6 open (H6o) and H7 closed (H7c) as found in the structure of holo InhA-NADH (PDB 1ENY, left); H6 closed (H6c) and H7 open (H7o) as in the structure of InhA-NAD⁺-PT70 (PDB 2X22 ligand ID TCU, chain A, right). The SBL, encompassed by helices H6 and H7, is depicted in light orange. The A and B loops are in yellow and red, respectively. The NADH/NAD⁺ (green) and the ligand (cyan) molecules, as well as the catalytic triad (magenta, see text), are shown as sticks. Distances used as indicators are shown as black dashed lines. The Ca atoms of targeted residues are shown as dark gray spheres. B) Box plot showing the distribution of the distance between Gly104 and Gly204 as a function of the conformational state of helix H6. C) Box plot showing the distribution of the distance between Ala157 and Ala211 as a function of the conformational state of helix H7. c, closed; i, intermediate; o, open (chains with disordered segments in H6 and H7 were excluded). Median and average values are indicated by a line and a cross, respectively. Lower and upper edges of the box correspond to lower and upper quartiles, respectively. Circles correspond to outliers. The number of occurrences (n) is also given.

distances could not be measured due to missing residues, that is, where segments of H6 (67 chains) and H7 (39 chains) are found disordered. However, it should be noted that the term “disordered” is used here without distinction whatever the degree of disorder observed, from partial to total.

Figure S2 (Supporting Information) provides a detailed picture of the ensemble of conformations adopted by helices H6 and H7 for the different chains in all wild-type MTB-InhA structures from the PDB. For instance, in the structure of the apo-form (6 chains), H6 is either open or disordered, whereas H7 is closed, intermediate, or disordered. In all 5 structures of the holoform of MTB-InhA (1 chain per structure), the H6 helix is in an open conformation, whereas H7 is closed. Thus, it seems that cofactor binding somehow stabilizes the SBL loop. With regard to the sole structure resolved for an MTB-InhA complex with the cofactor (NAD⁺) and a substrate analogue (6 chains), H6 and H7 are in open and closed/intermediate conformations, respectively. However, the opening of H6 (resp. the closing

of H7) is more (resp. less) pronounced for chains where the analog is bound compared to those where it is not present. As for complexes with inhibitors, all conformations are observed, albeit at varying frequencies. The next step was to establish whether any correlation exists between the conformations of H6 and H7 within each chain. This analysis was carried out for the ternary enzyme-cofactor-inhibitor complexes, which revealed several interesting features (Table 2).

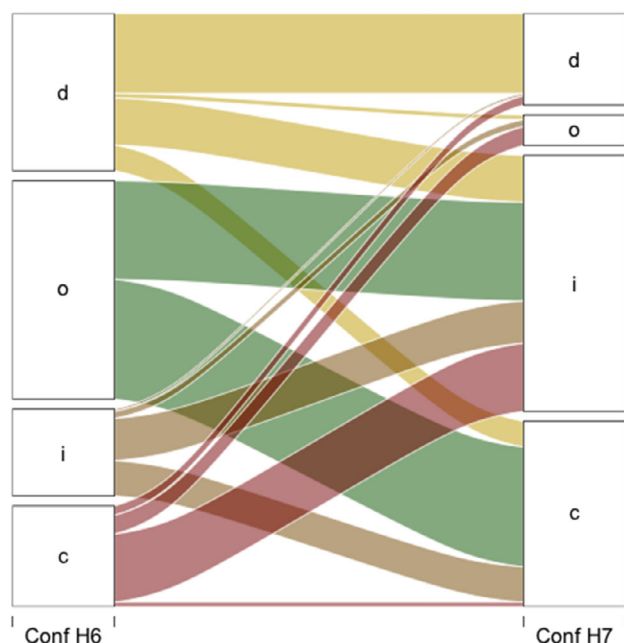
First, the closed conformation of H6 is only observed in the simultaneous presence of NAD⁺ and a bound ligand. Second, the closed conformation of H7 is mainly found for ligand-populated chains, but in this case independently of the cofactor's redox state. Third, when H6 (resp. H7) is closed, H7 (resp. H6) is most often—that is, apart from two exceptions—in an intermediate or open conformation, so that the closed states of H6 and H7 appear to be mutually exclusive. Fourth, the same applies to the coexistence of the open forms of H6 and H7 although the opening of H7 is not very frequent and, as for H6 closed, in

Table 2. Intra-chain analysis of the conformational states of helices H6 and H7 in the structures of ternary enzyme-cofactor-inhibitor complexes of wild-type MTB-InhA as a function of the redox state of the cofactor and ligand occupancy.

	H6c ^{a)}		H6i		H6o		H6d		Total
H7c ^{b)}	0 ^{c)}	0 ^{c)}	4	0	19	1	3	0	27
	2 ^{c)}	0 ^{c)}	9	0	7	2	3	0	23
H7i	0	0	2	0	10	6	2	2	22
	29	0	16	0	9	7	5	1	67
H7o	0	0	0	0	0	0	0	0	0
	8	0	2	0	0	0	2	0	12
H7d	0	0	0	0	0	0	4	2	6
	4	0	1	0	0	0	12	6	23
Total	43	0	34	0	45	16	31	11	180 ^{c)}

^{a)}The different conformations of H6 are given horizontally. ^{b)}The different conformations of H7 are given vertically. Letters c, i, o, and d refer to closed, intermediate, open, and disordered, respectively. ^{c)}The 180 individual chains of the 52 PDB structures of ternary enzyme-cofactor-inhibitor complexes were analyzed. For each pair of conformations (H6, H7), the number of occurrences (i.e., chains) is given in four squares. Top/bottom squares correspond to the number of chains for complexes obtained in the presence of NADH (gray filling)/NAD⁺ (no filling), whereas left/right squares correspond to the number of chains for which inhibitor binding was (in bold)/was not (in italics) observed.

the simultaneous presence of NAD⁺ and a bound ligand. Fifth and last, disorder of H7 is often (i.e., 83% of cases) accompanied by disorder of H6. The alluvial diagram on **Figure 2** shows the interrelation between the conformations of H6 and H7 for all chains of all wild-type MTB-InhA structures and illustrates that the same trends are observed.

**Figure 2.** Alluvial plot depicting the interrelation between the conformations of H6 (left) and H7 (right) in the SBL of wild-type MTB-InhA. Flows represent the proportion of chains with a given H6/H7 conformation (c, closed; i, intermediate; o, open; d, disordered). Colors correspond to the different conformations of H6.

We wanted to address whether any bias in the structural features described above could be introduced due to the crystallographic method itself, and especially by crystal packing, that is, contacts established between the different molecules making up the crystal. Concerning the structures of complexes comprising chains not occupied by a ligand (i.e., 38 chains corresponding to 13 different structures), half of them were obtained by cocrystallization and the other half by soaking. This rules out total dependence on the method of crystal preparation. When soaking was used, we also checked that, in the majority of cases, the active sites of the unoccupied chains are not blocked due to the crystal environment. We also checked that the different conformational states of H6 and H7 were not influenced by crystal packing. For this, we computed differences in accessible surface area (Δ ASA) due to crystal contacts for the residues corresponding to the two helices. The total absence of crystalline contact should correspond to a Δ ASA value of 0 Å², while the more negative the Δ ASA value, the greater the number of contacts with symmetric molecules. In addition, closed conformations might be expected to be the most sensitive to crystal packing effects. As shown in Figure S3 (Supporting Information), the conformations adopted by H6 and H7 do not seem to be totally dependent on crystal contacts. Figures S4 and S5 (Supporting Information) illustrate this point for the closed conformations of H6 and H7, respectively. However, this analysis does not allow us to assert that there is no structure where the SBL conformation is constrained by crystal packing. It does, however, suggest that the crystallographic bias—if any—would not be systematic.

2.3. Some Considerations on the Active Site of InhA

The InhA active site forms a deep cleft delineated by amino acid residues that contribute to the binding of NAD as well as substrates and inhibitors (**Figure 3A**, left). It includes the catalytic triad Phe149–Tyr158–Lys165, which plays a key role in cofactor binding, stabilizing the transition state/enolate intermediate, and proton transfer. The substrate-binding site itself can be subdivided into three distinct sites, referred to as sites I, II, and III (**Figure 3A**, right). Site I corresponds to the catalytic site where the reduction reaction takes place. Site II corresponds to a hydrophobic pocket, where the substrate's aliphatic chain is housed, and points towards the so-called minor portal.^[7b] Site III, exposed to solvent, corresponds to the entrance of the protein on the side of the major portal.^[7b] Interestingly, from one InhA structure to another, the side chains of Phe149 and Tyr158 can adopt two conformations, called *in* and *out*, depending on whether they point towards the protein interior or away from it, that is, towards the SBL. For example, in the InhA·NADH structure, both side chains are in the *out* conformation (**Figure 1A**, left), whereas binding of the substrate analogue rotates the Tyr158 side chain into the *in* conformation (**Figure 3A**, left).

2.4. The Long Quest for InhA Inhibition

The first structure of an inhibited form of InhA was that of the complex with INH-NADH obtained by preincubating the enzyme,

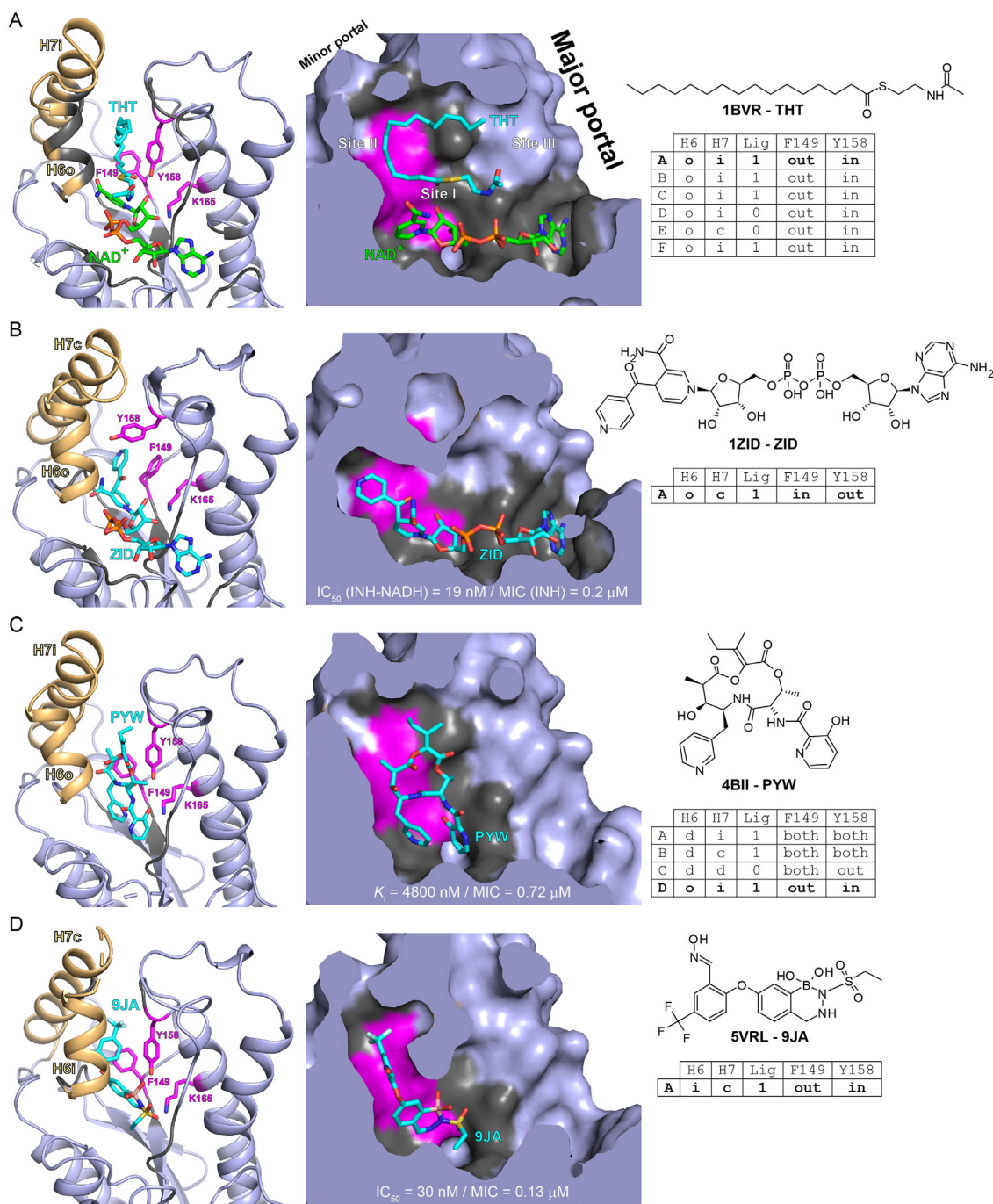


Figure 3. The InhA active site and the mode of binding of competitive inhibitors. A) Structure of MTB-InhA in complex with NAD⁺ and a C16 fatty acyl substrate analogue (PDB 1BVR, ligand ID THT, chain A). B) Structure of MTB-InhA in complex with INH-NADH (PDB 1ZID, ligand ID ZID, chain A). C) Structure of MTB-InhA in complex with pyridomycin (PDB 4BII, ligand ID PYW, chain D). D) Structure of MTB-InhA in complex with AN12855 (PDB 5VRL, ligand ID 9JA, chain A). On the left panels, the protein is shown as a light blue cartoon with the SBL in light orange. The NAD⁺ (green), the substrate analogue or the inhibitors (cyan), and the catalytic triad (magenta) are shown as sticks. Residues, other than the catalytic triad, within 5 Å of the cofactor or the substrate analogue/inhibitors are in gray. Indices c, i, and o refer respectively to the closed, intermediate, and open conformations of H6 and H7. The panels on the right correspond to cross-sections (viewed perpendicularly to the panels on the left) of the molecular surface. Inhibition parameters available in the literature are given: IC₅₀, half-maximal inhibitory concentration; K_i, inhibition constant; MIC, minimum inhibitory concentration (note: given values are indistinctly for either 50%, 99%, or total inhibition). Right panel inserts include the chemical structure, PDB code, and ligand identifier and indicate for each chain the conformation of helices H6 and H7, the presence (1) or absence (0) of the ligand, and the orientation of residues Phe149 and Tyr158. In bold, chain displayed on the figure.

the cofactor and the inhibitor in the presence of MnCl₂ (Figures 3B and S6A, Supporting Information).^[19] This structure could be repeated by soaking of crystals of InhA-NADH in a solution of the preformed active metabolite of INH (Figure S6A,

Supporting Information).^[7a] Structures of MTB-InhA preincubated with competitive adducts of the cofactor were also obtained with thioamide analogues of INH, that is, the second-line drugs ethionamide (ETH) and prothionamide (PTH),^[20] or with INH-NADP

(Figure S6A, Supporting Information).^[21] All these structures revealed that the open 4S-ketoamide forms of the adducts are present in the active site. All structures but the one corresponding to PTH-NADH contain 1 molecule in the a.u. (meaning the InhA tetramer obeys crystallographic symmetry) where H6 is open and H7 is closed. Interestingly, the MTB-InhA-PTH-NADH structure contains 2 molecules in the a.u., one with also H6 open and H7 closed (Figure S6A, Supporting Information) and the other with H6 intermediate and H7 open (Figure S6B, Supporting Information). This is a typical example where the SBL conformation can be under the influence of crystal packing (or vice versa?). In all structures, the orientation of Phe149 is displaced from the *out* conformation, as observed in the structure of InhA-NADH (Figure 1A), to the *in* conformation to avoid steric conflict and allow stacking interaction with the pyridine moiety of the adducts.

Given that compounds leading to cofactor adduct inhibitors are prodrugs that require activation, thus inducing frequent resistance phenomena, massive work has been carried out to overcome this problem by identifying direct inhibitors of InhA. A direct competitive inhibitor of NADH binding in InhA is the natural compound pyridomycin.^[16a] Structures of InhA-pyridomycin were obtained by soaking crystals of wild-type InhA-NAD⁺ or InhA^{S94A}-NADH.^[22] They revealed how the inhibitor not only mimics the cofactor, in particular the nicotinamide nucleotide half, but also occupies part of the substrate-binding site on sites I and II (Figure 3C). For the structure with the wild-type enzyme, there are 4 molecules in the a.u. showing different occupancies of the cofactor and/or pyridomycin. In all 4 molecules, H6 is open or disordered, and H7 is closed, intermediate, or disordered. When only pyridomycin is bound, H6 is open, H7 is in the intermediate conformation, and the orientation of Tyr158 is rotated from the *out* to the *in* conformation to avoid steric conflict with the inhibitor (Figure 3C). Diazaborines form another class of competitive inhibitors that also compete with both the cofactor and the substrate as exemplified by the structure with the lead compound AN12855 (Figure 3D).^[23] Crystals of InhA-AN12855 were obtained by cocrystallization and contain 1 molecule per a.u. in which H6 is in an intermediate conformation, H7 is closed, Phe149 is *out*, and Tyr158 is *in*. The AN12855-binding mode to InhA is reminiscent of pyridomycin binding in terms of both position (Figure 3D) and interaction pattern (not shown).

All other developed direct InhA inhibitors bind to the enzyme in the presence of the cofactor. Among them, the diaryl ether molecules form the most studied family. Indeed, of the 78 crystallographic structures of wild-type MTB-InhA in the PDB, 28 (i.e., one third) correspond to complexes with such ligands.^[24] The first diaryl ether inhibitor identified, the broad spectrum antimicrobial triclosan (TCL), revealed to be uncompetitive with respect to NAD⁺ and exhibits an IC₅₀ of 1 μ M.^[24d,24i] The structure of the MTB-InhA-NAD⁺-TCL complex was obtained by cocrystallization and contains 2 differently populated InhA molecules per a.u.^[24d] Two TCL molecules fully occupy the substrate-binding site in chain A—TCL1, stacked with the nicotinamide ring of the cofactor in site I, and TCL2, positioned in hydrophobic site II—and H6 and H7 of the SBL are in open and intermediate conformations, respectively (Figure 4A). In contrast, only TCL1 was found in chain B,

where H6 is closed, and H7 is open (Figure S7, Supporting Information). It is noteworthy that the closed conformation of H6 in chain B is another example of SBL conformation under the influence of/influencing crystal packing. Based on this structure, several diaryl ether derivatives were designed with various alkyl chain lengths, mimicking the lipidic substrate (recently reviewed in^[24j]). Among these derivatives, the 8PP compound bearing a C8-alkyl chain at position 5 showed the best inhibition with an IC₅₀ of 5 nM.^[24i] The structure of the InhA-NAD⁺-8PP has been solved (Figure 4B). Of the 8 molecules in the a.u., only 2 of them are populated with the inhibitor, all have H6 disordered, and H7 is either disordered or intermediate independently of ligand binding or not. The 8PP diaryl ether moiety shares the same binding mode as TCL1, and its alkyl chain occupies site II towards the minor portal (Figure 4B). A broad range of diaryl ether analogues were further developed to target InhA.^[25] This includes molecules where the alkyl chain has been substituted for a triazole, which opened the route to explore a variety of substitutions by click chemistry.^[24h,25] Several structures corresponding to triazole-based diaryl ethers with different substituents have been resolved after cocrystallization with InhA-NAD⁺, for example with a cyclopropyl on the triazole at position 5 and a methyl at position 2' (Figure 4C).^[24h] Although these structures were obtained in different space groups, with 1 to 8 molecules per a.u., all chains have H6 closed or intermediate and H7 intermediate, whether they are involved in crystalline contacts or not. These triazole-bearing molecules have been shown to display increased protein residence time on the protein, a feature thought to enhance drug efficacy,^[26] and improved antimycobacterial activity overall.^[24h] The subsequent development of new diaryl ether-based inhibitors then aimed to better explore the enzyme's active site. Using a molecular hybridization approach, a series of triazole-based diaryl ethers bearing various heterocycles, mainly coumarins, were developed. These compounds exhibited good inhibitory activity against the enzyme (submicromolar to nanomolar range) and in vitro antimycobacterial activity.^[24a] X-ray structures of InhA-NAD⁺ cocrystallized with two of these coumarin derivatives revealed how these compounds can protrude in the minor portal in an unprecedented way (Figure 4D).^[24a] In these two structures, all 4 chains of the a.u. are populated with the ligand and have H6 closed and H7 intermediate. The introduction of a pyridone in the 4'-position of an alkylated diaryl ether, such as compound SKTS1, has enabled exploration of the active site on the major portal side at site III.^[24b] In the structure of the corresponding complex obtained by cocrystallization in the presence of InhA-NAD⁺, which contains 1 molecule per a.u., helix H6 and H7 are in intermediate and closed conformations, respectively (Figure 4E).

Besides diaryl ethers, several other direct inhibitors of InhA have been discovered and developed, and their interaction with the enzyme is structurally characterized. These include aryl-carboxamides,^[24d,27] such as the Genz-10850 compound identified and evaluated at the same time as TCL.^[24d] The structure of the ternary complex formed between InhA-NADH and Genz-10850—the best aryl-carboxamide compound with an IC₅₀ = 160 nM—revealed that the inhibitor nicely fits in the substrate-binding site at sites I and II (Figure 5A).^[24d] It contains 6 molecules per a.u., only 4 with a bound ligand, but all with H6 open and H7

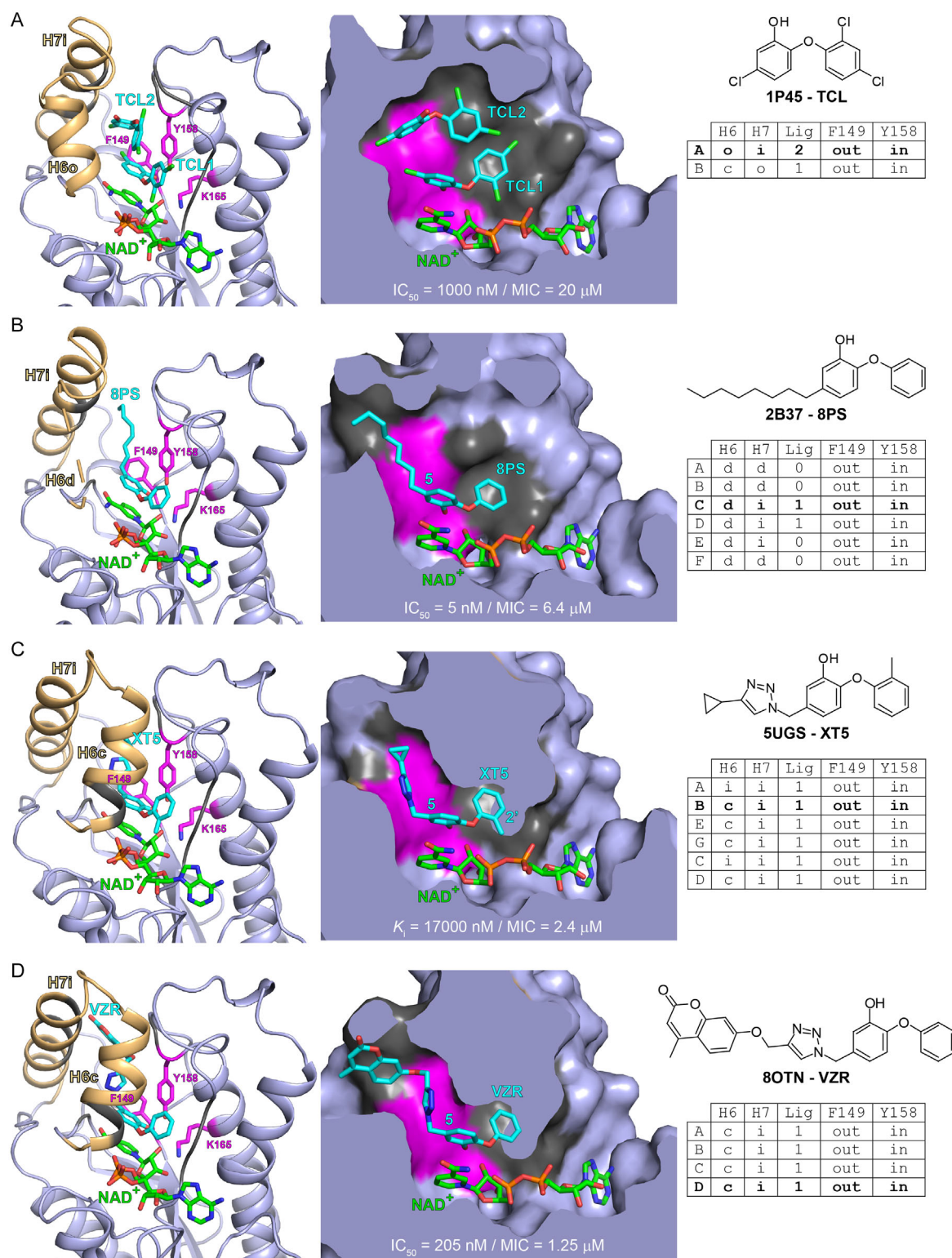


Figure 4. Binding of diaryl ether inhibitors to MTB-InhA. A) Complex with NAD⁺ and triclosan (PDB 1P45, ligand ID TCL, chain A). B) Complex with NAD⁺ and compound 8PP (PDB 2B37, ligand ID 8PS, chain C). C) Complex with NAD⁺ and compound PT501 (PDB 5UGS, ligand ID XT5, chain B). D) Complex with NAD⁺ and compound 7b (PDB 8OTN, ligand ID VZR, chain D). E) Complex with NAD⁺ and compound SKT51 (PDB 6YUU, ligand ID F9T, chain A). On the left panels, the protein is shown as a light blue cartoon with the SBL in light orange. The NAD⁺ (green), the inhibitors (cyan), and the catalytic triad (magenta) are shown as sticks. Residues, other than the catalytic triad, within 5 Å of the cofactor or inhibitors are in gray. The substituted positions on the diaryl ether scaffold are labeled. Indices c, i, o, and d refer respectively to the closed, intermediate, open, and disordered conformations of H6 and H7. The panels on the right correspond to cross-sections (viewed perpendicularly to the panels on the left) of the molecular surface. Inhibition parameters available in the literature are given: IC_{50} , half-maximal inhibitory concentration; K_i , inhibition constant; MIC, minimum inhibitory concentration (note: given values are indistinctively for either 50%, 99%, or total inhibition). Right panel inserts include the chemical structure, PDB code, and ligand identifier and indicate for each chain the conformation of helices H6 and H7, the presence (1 or 2) or absence (0) of the ligand, and the orientation of residues Phe149 and Tyr158. In bold, chain displayed on the figure.

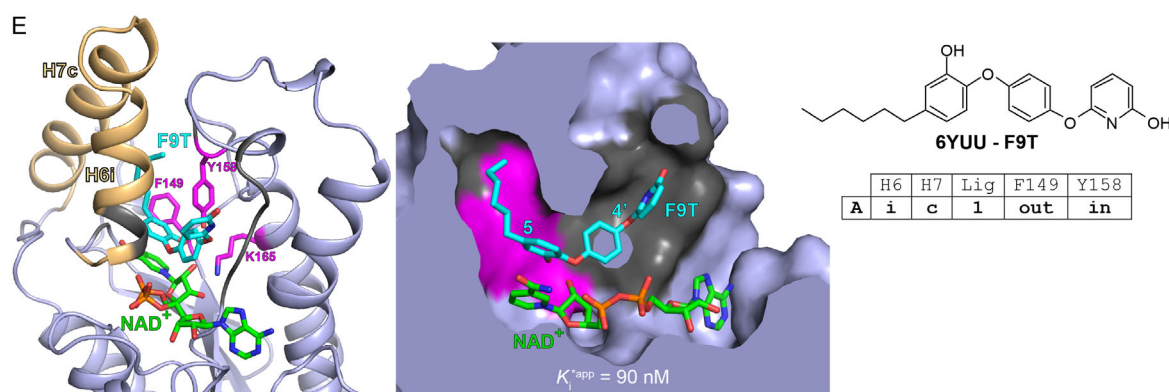


Figure 4. Continued.

either in closed or intermediate conformation. Carboxamide derivatives containing pyrrolidines or pyrazoles or both have also been developed with IC_{50} in the submicromolar–nanomolar range.^[27a,c,28] Several structures of such complexes have been resolved in which the pyrazoles/pyrrolidines are differently oriented (Figures S8, Supporting Information). In these structures, the different chains in the a.u. have H6 open, intermediate, or disordered and H7 closed, intermediate, or disordered. Among these structures, the carboxamide derivative containing both pyrrolidine and pyrazole moieties exhibits a unique position, not found in any of the other InhA structures, where it points away from the substrate-binding site towards (and disrupts part of) helix H6 (Figure 5B). Other pyrazole-containing inhibitors of InhA are derivatives based on thiazole–thiadiazole pharmacophores with nanomolar activity against the enzyme.^[29] Characterization of these inhibitors revealed that they are uncompetitive with the cofactor but compete with the substrate at sites II and III as revealed by three X-ray structures (see for instance Figure 5C for compound GSK625).^[29] In all three structures, representing 14 chains (all populated with the ligand), H6 is open or intermediate and H7 is closed or intermediate (Figure 5A–C, right panel inserts). Pyridone derivatives constitute another class of compounds that block the substrate-binding site.^[30] These compounds have low micromolar activity against InhA, and the X-ray structures of two complexes, including the one with the lead candidate NITD-916,^[30] were determined also illustrating binding at sites I and II, with H6 and H7 always found in open and intermediate conformations, respectively (Figure 5D).

Direct inhibitors of InhA belonging to other chemical classes are discussed in the following in ascending chronological order of structure deposition in the PDB. This includes pyridazinones (two unpublished structures: PDB 4D0R and 4D0S), which form a linear scaffold occupying site I and piercing through site II, thereby causing Phe149 to flip from the *out* position to the *in* position (Figure 6A). Multiple chemical series, with IC_{50} from millimolar to submicromolar, were identified through screening of DNA-encoded chemical libraries,^[31] including other pyrazole derivatives than those described above. Structures were solved for crystals prepared by soaking with NADH and representatives of five series.^[31] One of the best inhibitors identified is based on a cyclohexyl ring. It occupies all three sites of the substrate

pocket and protrudes from the major portal in a unique manner (Figure 6B). Another quite unique manner of binding was found for a benzimidazole derivative identified by virtual screening and with submicromolar IC_{50} .^[32] The structure of the corresponding complex was obtained by soaking with InhA·NAD⁺ crystals and revealed that the compound mimics the substrate acyl chain at some distance from the cofactor, in the same way as TCL2, but also reaches the minor portal (Figure 6C).^[32] Using a fragment-based screening and growing approach, sulfonamide derivatives with submicromolar IC_{50} were developed.^[33] The crystal structure of one of them was solved after soaking in the presence of NAD⁺ and revealed binding at sites I and II (Figure 6D). Last, inhibition of InhA by 3-nitropropanoic acid with an IC_{50} value of 71 μM has been reported recently, and the corresponding structure was resolved by cocrystallization in the presence of NADH, where 3-nitropropanoic acid binds at site I (Figure 6E).^[34] Finally, a large number of studies have been carried out to develop InhA inhibitors, either by trying to improve the abovementioned molecules—in particular triclosan analogues—or by using new scaffolds. These studies, which incorporate *in silico* approaches (virtual screening/molecular docking), are too numerous to be included in the bibliography of this article (for a review, see for instance^[35]).

2.5. Is it Crystal Clear?

The aim of this article was not to describe in detail the atomic interactions between InhA, its cofactor, and the ligands for which so many crystallographic structures have been solved. The position of the cofactor itself is invariant, and the greatest conformational variations in the extended form it adopts are confined to the dihedral angles of the pyrophosphate group (which contains most of NAD's rotatable bonds) and to a very lesser extent around the C3–C7 bond of nicotinamide, while ribose puckering fluctuates very little. Linked by two hydrogen bonds to the hydroxyl groups of the nicotinamide ribose, the conformation of Lys165 also fluctuates very little and is even conserved in the absence of a cofactor, that is, in the apo form of the enzyme. For the other two catalytic residues (Phe149 and Tyr158), their *in* or *out* conformation is dependent on steric hindrance in the active site. Phe149, in its *out* conformation, plays a crucial role in cofactor binding to induce the proper conformation of the nicotinamide.

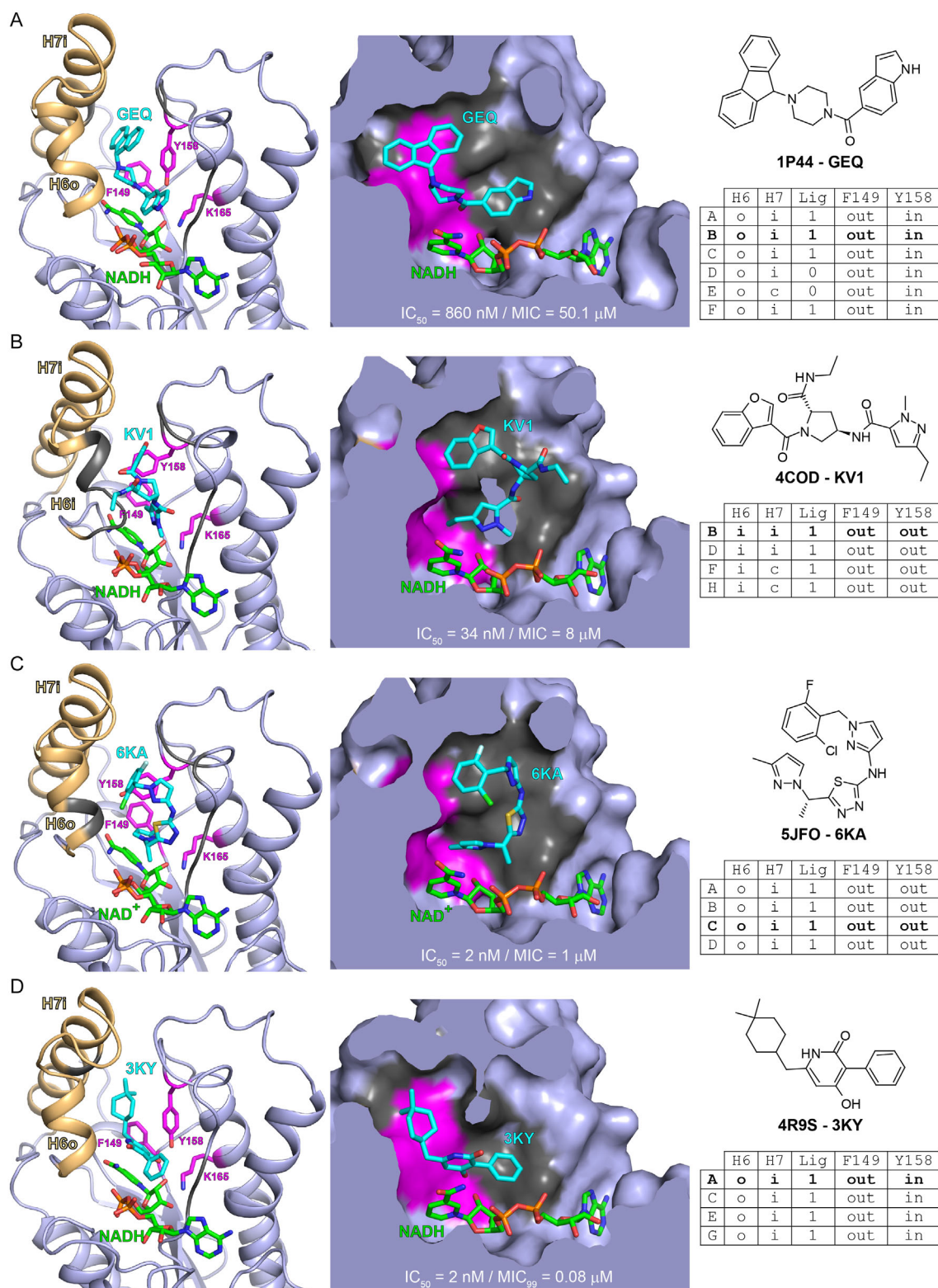


Figure 5. Binding of carboxamide-, diathiamide-, and pyridone-based inhibitors to MTB-InhA. A) InhA·NADH·Genz-10850 (PDB 1P44, ligand ID GEQ, chain B). B) InhA·NADH·pyrrolidine/pyrazole-carboxamide (PDB 4COD, ligand ID KV1, chain B). C) InhA·NADH·GSK625 (PDB 5JFO, ligand ID 6KA, chain C). D) InhA·NADH·NITD-916 (PDB 4R9S, ligand ID 3KY, chain A). On the left panels, the protein is shown as a light blue cartoon with the SBL in light orange. The NADH/NAD⁺ (green), the inhibitors (cyan), and the catalytic triad (magenta) are shown as sticks. Residues, other than the catalytic triad, within 5 Å of the cofactor or inhibitors are in gray. Indices c, i, and o refer respectively to the closed, intermediate, and open conformations of H6 and H7. The panels on the right correspond to cross-sections (viewed perpendicularly to the panels on the left) of the molecular surface. Inhibition parameters available in the literature are given: IC₅₀, half-maximal inhibitory concentration; MIC, minimum inhibitory concentration (note: given values are indistinctively for either 50%, 99%, or total inhibition). Right panel inserts include the chemical structure, PDB code, and ligand identifier and indicate for each chain: the conformation of helices H6 and H7, the presence (1) or absence (0) of the ligand, and the orientation of residues Phe149 and Tyr158. In bold, chain displayed on the figure.

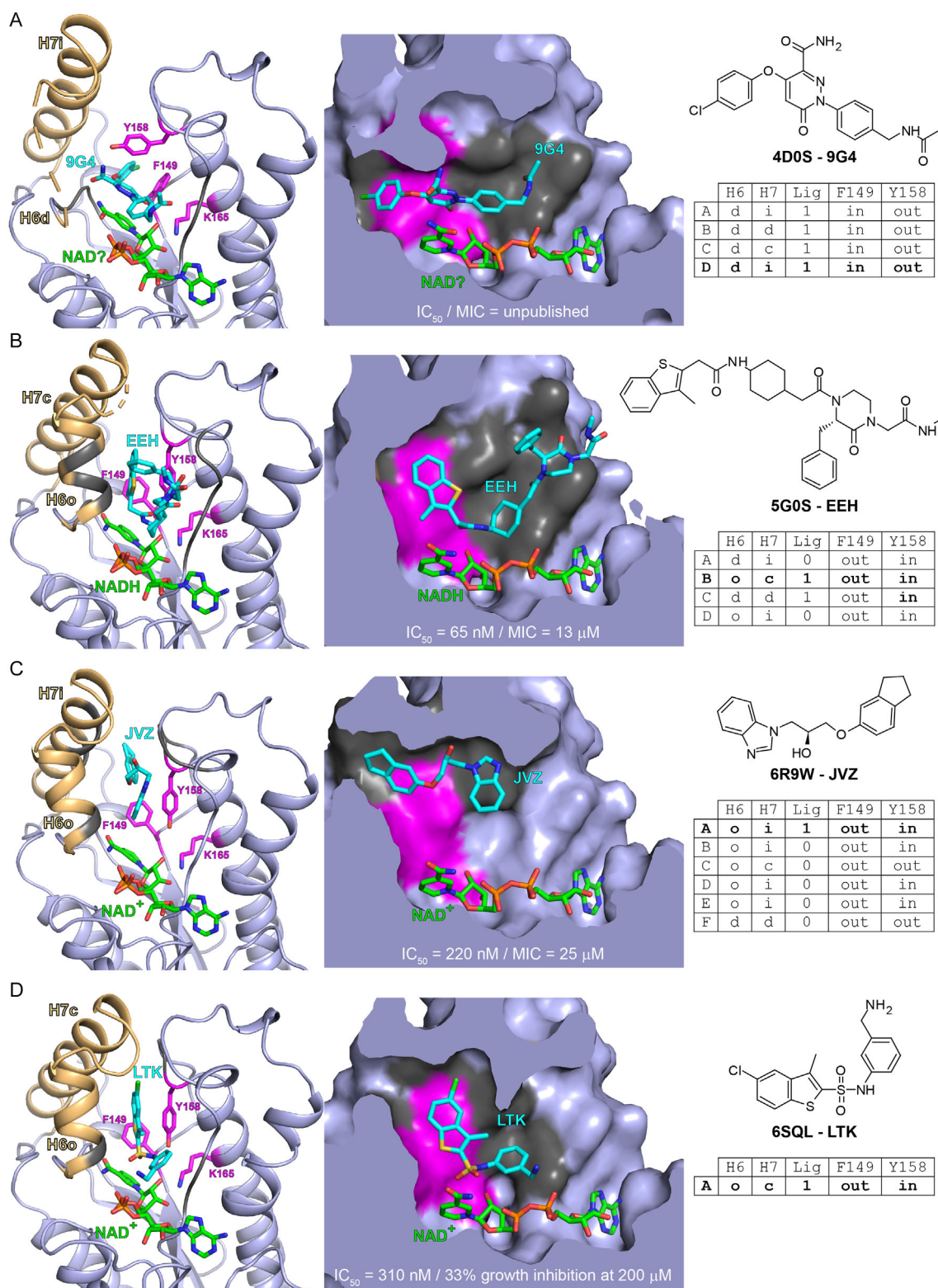


Figure 6. Binding of other inhibitors to MTB-InhA. A) InhA-NAD⁺·pyridazinone (PDB 4D0S, ligand ID 9G4, chain D). B) InhA-NADH-cyclohexyl derivative (PDB 5G0S, ligand ID EEH, chain B). C) InhA-NAD⁺·benzimidazole derivative (PDB 6R9W, ligand ID JVZ, chain A). D) InhA-NAD⁺·sulfonamide derivative (PDB 6SQL, ligand ID LTK, chain A). E) InhA-NAD⁺·nitropropanoic acid (PDB 7E48, ligand ID 3NP, chain A). On the left panels, the protein is shown as a light blue cartoon with the SBL in light orange. The NADH/NAD⁺/NAD[?] (green), the inhibitors (cyan), and the catalytic triad (magenta) are shown as sticks. Residues, other than the catalytic triad, within 5 Å of the cofactor or inhibitors are in gray. Indices c, i, o, and d refer respectively to the closed, intermediate, open, and disordered conformations of H6 and H7. The panels on the right correspond to cross-sections (viewed perpendicularly to the panels on the left) of the molecular surface. Inhibition parameters available in the literature are given: IC₅₀, half-maximal inhibitory concentration; MIC, minimum inhibitory concentration (note: given values are indistinctively for either 50%, 99%, or total inhibition). Right panel inserts include the chemical structure, PDB code, and ligand identifier and indicate for each chain: the conformation of helices H6 and H7, presence (1) or absence (0) of the ligand, and the orientation of residues Phe149 and Tyr158. In bold, chain displayed on the figure.

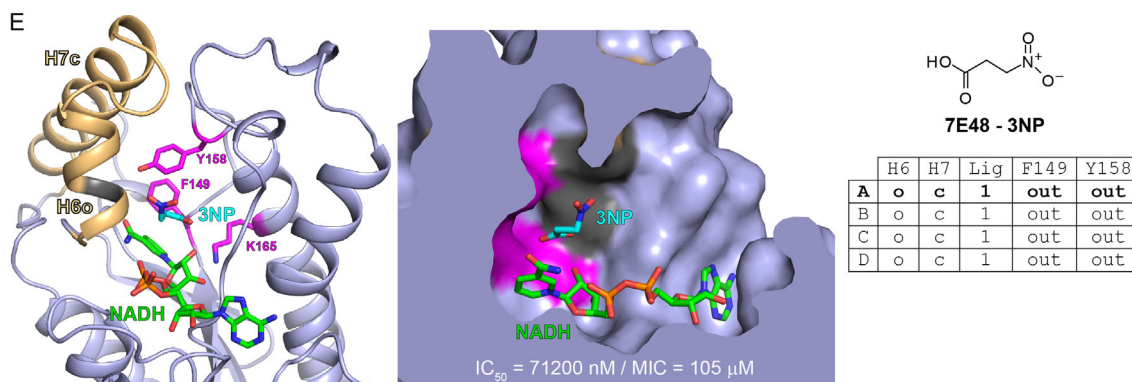


Figure 6. Continued.

The *in* conformation is only observed in the complexes with cofactor adduct inhibitors (Figure 3B and S6, Supporting Information) and in the complex with a pyridazinone (Figure 5A), representing 13/240 chains for 8/78 structures. In these structures, H6 is predominantly open or disordered, and H7 is closed, intermediate, or disordered (Table S2, Supporting Information). The *in* and *out* conformations of Tyr158 are more widely distributed. The *in* conformation is found in 158 chains and 46 structures, compared with 73 chains and 30 structures for the *out* conformation, and 9 chains in 6 structures where alternate *in/out* conformations were observed. Tyr158 switches from the *out* conformation in the holo form to the *in* conformation upon substrate binding (Figure 3A) and also with inhibitors that occupy site II, such as diaryl ether derivatives (Figure 4). It is also accepted that Tyr158 plays an important role in the InhA-catalyzed reduction mechanism, stabilizing the enolate intermediate. However, it has recently been shown that this residue may also play an important role in substrate positioning for the stereo-specific reaction.^[36] It should be noted that a wide variety of H6 and H7 conformations is observed whatever the orientation of Tyr158 (Table S2, Supporting Information). Yet, when H6 is closed or intermediate, and independently of the orientation of H7, Tyr158 is *in* (whereas as indicated above Phe149 is *out*). This applies in particular—but not exclusively—to inhibitors of the diaryl ether family and exclusively to these when the analysis is restricted to H6 closed. Diaryl ethers interact with Tyr158 via their phenol group, and several studies carried out by Peter J. Tonge et al. have shown that they inhibit InhA via a two-step induced-fit mechanism, with the H6 helix switching from the open to the closed conformation.^[36,37] Depending on the steric hindrance caused by the substitution in position 5, these molecules could be either “rapid-reversible” or “slow-onset” inhibitors, with a potential gain in residence time for the latter, where the H6 helix is respectively open or closed. However, as indicated by these authors and in our previous review,^[12a] the present analysis confirms that for the same compound, several conformations can be sampled by the different chains found in the a.u. of the corresponding structure (Figure 4, right panel inserts). Finally, the interrelation between the conformations of helices H6 and H7 (see Figure 2) has so far been little studied, except in an article by Peter J. Tonge’s team, which proposed a system similar to a coin purse ball clasp that will not be detailed here.^[37f]

3. Conclusion

Since the discovery of InhA as the main target of isoniazid, and after more than 20 years dedicated to the discovery and design of direct inhibitors to avoid resistance problems, some of which have very good IC₅₀ or K_i, or even MIC, no molecule of this type is used, or even being tested, in the clinic (to the best of our knowledge). The detailed analysis of all MTB-InhA crystallographic structures presented here has established a number of very specific traits of this enzyme in terms of structure–dynamics–activity relationships. These could be integrated to complement the numerous molecular dynamics and molecular docking studies that have been carried out on the protein.^[12b,18b,38] However, this is a first step, and to make further progress, we believe it is absolutely essential to carry out a purely statistical analysis on the descriptors we derived from the PDB. Despite the challenge this represents, it is even more essential that this be done at the level of the quaternary structure of the enzyme to identify possible allosteric sites and also because of its possible involvement in a wider network of interactions within FAS-II.^[13a,14] From an experimental point of view, InhA is a very attractive biological object to be studied by techniques such as cryo-electron microscopy (cryo-EM) as well as, at room temperature, serial femtosecond crystallography (SFX) or serial synchrotron crystallography (SSC). These techniques could be of great help in revealing conformational ensembles and structural changes upon ligand (cofactor, substrate, and inhibitor) binding, since NMR unfortunately cannot be used for size reasons.^[39] Taking all these aspects into account may lead to the development of molecules that are more and more active on the enzyme and effective against the tubercle bacillus, this second stage being another huge challenge in itself.

4. Experimental Section

All structural information was extracted from the Protein Data Bank (<http://www.rcsb.org/>).^[40] Structure superimposition and calculation of accessible surface areas were respectively performed using the programs superpose^[41] and areaimol^[42] as implemented in the CCP4 software suite.^[43] The PyMOL Molecular Graphics System, Version 3.1.0 Schrödinger, LLC, and Coot^[44] were used for structural inspection and analysis. Figures of protein structures were prepared using PyMOL. The alluvial plot was carried out in the R environment

(v. 4.2.1)^[45] with the RStudio interface (v. 2024.9.0.375),^[46] using the alluvial (v. 0.1-2) library.^[47]

Acknowledgements

This project has received funding from the Agence Nationale de la Recherche (ANR-23-CE44-0002) to C.L. and L.M. The authors would like to thank the scientific staff at the European Synchrotron Radiation Facility (Grenoble, France), SOLEIL (Gif sur Yvette, France) and ALBA (Barcelona, Spain), where their own crystallographic experiments on InhA were carried out.

Conflict of Interest

The authors declare no conflict of interest.

Data Availability Statement

The data that support the findings of this study are available from the corresponding author upon reasonable request.

Keywords: InhA • inhibitors • *Mycobacterium tuberculosis* • rational drug design • X-ray crystallography

- [1] J. F. Murray, D. E. Schraufnagel, P. C. Hopewell, *Ann. Am. Thorac. Soc.* **2015**, *12*, 1749.
- [2] WHO operational handbook on tuberculosis. Module 4: Treatment – drug-susceptible tuberculosis treatment, World Health Organization, Geneva **2022**.
- [3] A. Banerjee, E. Dubnau, A. Quemard, V. Balasubramanian, K. S. Um, T. Wilson, D. Collins, G. de Lisle, W. R. Jacobs, *Science* **1994**, *263*, 227.
- [4] a) K. Takayama, L. Wang, L. David Hugo, *Antimicrob. Agents Chemother.* **1972**, *2*, 29; b) F. G. Winder, P. B. Collins, *Microbiology* **1970**, *63*, 41.
- [5] a) H. Marrakchi, G. Lanéeelle, A. Quémard, *Microbiology* **2000**, *146*, 289; b) A. Quemard, J. C. Sacchettini, A. Dessen, C. Vilchère, R. Bittman, W. R. Jacobs Jr., J. S. Blanchard, *Biochemistry* **1995**, *34*, 8235.
- [6] A. Dessen, A. Quémard, J. S. Blanchard, W. R. Jacobs, J. C. Sacchettini, *Science* **1995**, *267*, 1638.
- [7] a) A. Chollet, L. Mourey, C. Lherbet, A. Delbot, S. Julien, M. Baltas, J. Bernadou, G. Pratiel, L. Maveyraud, V. Bernardes-Génisson, *J. Struct. Biol.* **2015**, *190*, 328; b) D. A. Rozwarski, C. Vilchère, M. Sugantino, R. Bittman, J. C. Sacchettini, *J. Biol. Chem.* **1999**, *274*, 15582.
- [8] a) P. Lempens, C. J. Meehan, K. Vandellannoote, K. Fissette, P. de Rijk, A. Van Deun, L. Rigouts, B. C. de Jong, *Sci. Rep.* **2018**, *8*, 3246; b) J. N. Torres, L. V. Paul, T. C. Rodwell, T. C. Victor, A. M. Amallraja, A. Elghraoui, A. P. Goodmanson, S. M. Ramirez-Busby, A. Chawla, V. Zadorozhny, E. M. Streicher, F. A. Sirgel, D. Catanzaro, C. Rodríguez, M. T. Gler, V. Crudu, A. Catanzaro, F. Valafar, *Emerg. Microbes Infect.* **2015**, *4*, 1; c) C. Vilchère, R. Jacobs William, *Microbiol. Spectr.* **2014**, *2*, <http://10.1128/microbiolspec.mgm1122-0014-2013>.
- [9] Global Tuberculosis Report 2024, World Health Organization, Geneva **2024**.
- [10] A. Negi, S. Perveen, R. Gupta, P. P. Singh, R. Sharma, *J. Med. Chem.* **2024**, *67*, 2264.
- [11] H. Marrakchi, M.-A. Lanéeelle, M. Daffé, *Chem. Biol.* **2014**, *21*, 67.
- [12] a) A. Chollet, L. Maveyraud, C. Lherbet, V. Bernardes-Génisson, *Eur. J. Med. Chem.* **2018**, *146*, 318; b) M. Boff de Avila, G. Bitencourt-Ferreira, W. F. de Azevedo, *Curr. Med. Chem.* **2020**, *27*, 745.
- [13] a) N. A. Kruh, R. Rawat, B. P. Ruzsicska, P. J. Tonge, *Protein Sci.* **2007**, *16*, 1617; b) H. Marrakchi, S. Ducasse, G. Labesse, H. Montrozier, E. Margeat, L. Emorine, X. Charpentier, M. Daffé, A. K. Quémard, *Microbiology* **2002**, *148*, 951.
- [14] R. Veyron-Churlet, O. Guerrini, L. Mourey, M. Daffé, D. Zerbib, *Mol. Microbiol.* **2004**, *54*, 1161.
- [15] H. T. Kim, S. Kim, B. K. Na, J. Chung, E. Hwang, K. Y. Hwang, *Biochem. Biophys. Res. Commun.* **2017**, *493*, 28.
- [16] a) R. C. Hartkoorn, C. Sala, J. Neres, F. Pojer, S. Magnet, R. Mukherjee, S. Uplekar, S. Boy-Röttger, K. H. Altmann, S. T. Cole, *EMBO Mol. Med.* **2012**, *4*, 1032; b) J. S. Oliveira, J. H. Pereira, F. Canduri, N. C. Rodrigues, O. N. de Souza, W. F. de Azevedo, L. A. Basso, D. S. Santos, *J. Mol. Biol.* **2006**, *359*, 646.
- [17] Y. Kallberg, U. Oppermann, H. Jörnvall, B. Persson, *Eur. J. Biochem.* **2002**, *269*, 4409.
- [18] a) R. F. Tarabini, L. F. S. M. Timmers, C. E. Sequeiros-Borja, O. Norberto de Souza, *Sci. Rep.* **2019**, *9*, 13683; b) A. L. da Costa, I. Pauli, M. Dorn, E. K. Schroeder, C. G. Zhan, O. N. de Souza, *J. Mol. Model.* **2012**, *18*, 1779.
- [19] a) M. V. B. Dias, I. B. Vasconcelos, A. M. X. Prado, V. Fadel, L. A. Basso, W. F. de Azevedo, D. S. Santos, *J. Struct. Biol.* **2007**, *159*, 369; b) D. A. Rozwarski, G. A. Grant, D. H. R. Barton, W. R. Jacobs, J. C. Sacchettini, *Science* **1998**, *279*, 98.
- [20] F. Wang, R. Langley, G. Gulten, L. G. Dover, G. S. Besra, W. R. Jacobs Jr., J. C. Sacchettini, *J. Exp. Med.* **2007**, *204*, 73.
- [21] A. Argyrou, M. W. Vetting, J. S. Blanchard, *J. Am. Chem. Soc.* **2007**, *129*, 9582.
- [22] R. C. Hartkoorn, F. Pojer, J. A. Read, H. Gingell, J. Neres, O. P. Horlacher, K.-H. Altmann, S. T. Cole, *Nat. Chem. Biol.* **2014**, *10*, 96.
- [23] Y. Xia, Y. Zhou, D. S. Carter, M. B. McNeil, W. Choi, J. Halladay, P. W. Berry, W. Mao, V. Hernandez, T. O'Malley, A. Korkegian, B. Sundel, L. Flint, L. K. Woolhiser, M. S. Scherman, V. Gruppo, C. Hastings, G. T. Robertson, T. R. Ioerger, J. Sacchettini, P. J. Tonge, A. J. Lenaerts, T. Parish, M. Alley, *Life Sci. Alliance* **2018**, *1*, e201800025.
- [24] a) M. Chebaiki, E. Delfourne, R. Tamhaev, S. Danoun, F. Rodriguez, P. Hoffmann, E. Grosjean, F. Goncalves, J. Azéma-Despeyroux, A. Pál, J. Korduláková, N. Preuilh, S. Britton, P. Constant, H. Marrakchi, L. Maveyraud, L. Mourey, C. Lherbet, *Eur. J. Med. Chem.* **2023**, *259*, 115646; b) S. Eltschkner, J. Kehrein, T. A. Le, S. Davoodi, B. Merget, S. Basak, J. D. Weinrich, J. Schiebel, P. J. Tonge, B. Engels, C. Sottriffer, C. Kisker, *ACS Infect. Dis.* **2021**, *7*, 746; c) J. S. Freundlich, F. Wang, C. Vilchère, G. Gulten, R. Langley, G. A. Schiehser, D. P. Jacobus, W. R. Jacobs Jr., J. C. Sacchettini, *ChemMedChem* **2009**, *4*, 241; d) M. R. Kuo, H. R. Morbidoni, D. Alland, S. F. Sneddon, B. B. Gourlie, M. M. Stavesky, M. Leonard, J. S. Gregory, A. D. Janjigian, C. Yee, J. M. Musser, B. Kreiswirth, H. Iwamoto, R. Perozzo, W. R. Jacobs Jr., J. C. Sacchettini, D. A. Fidock, *J. Biol. Chem.* **2003**, *278*, 20851; e) H.-J. Li, C.-T. Lai, P. Pan, W. Yu, N. Liu, G. R. Bommineni, M. Garcia-Diaz, C. Simmerling, P. J. Tonge, *ACS Chem. Biol.* **2014**, *9*, 986; f) S. R. Luckner, N. Liu, C. W. am Ende, P. J. Tonge, C. Kisker, *J. Biol. Chem.* **2010**, *285*, 14330; g) P. Pan, S. E. Knudson, G. R. Bommineni, H.-J. Li, C.-T. Lai, N. Liu, M. Garcia-Diaz, C. Simmerling, S. S. Patil, R. A. Slayden, P. J. Tonge, *ChemMedChem* **2014**, *9*, 776; h) L. A. Spagnuolo, S. Eltschkner, W. Yu, F. Daryae, S. Davoodi, S. E. Knudson, E. K. H. Allen, J. Merino, A. Pschibul, B. Moree, N. Thivalapill, J. J. Truglio, J. Salafsky, R. A. Slayden, C. Kisker, P. J. Tonge, *J. Am. Chem. Soc.* **2017**, *139*, 3417; i) T. J. Sullivan, J. J. Truglio, M. E. Boyne, P. Novichenok, X. Zhang, C. F. Stratton, H.-J. Li, T. Kaur, A. Amin, F. Johnson, R. A. Slayden, C. Kisker, P. J. Tonge, *ACS Chem. Biol.* **2006**, *1*, 43; j) R. Tamhaev, E. Grosjean, H. Ahamed, M. Chebaiki, F. Rodriguez, D. Recchia, G. Degiacomi, M. R. Pasca, L. Maveyraud, L. Mourey, C. Lherbet, *Bioorg. Chem.* **2024**, *143*, 107032.
- [25] J. Stec, C. Vilchère, S. Lun, A. L. Peryman, X. Wang, J. S. Freundlich, W. Bishai, W. R. Jacobs Jr., A. P. Kozikowski, *ChemMedChem* **2014**, *9*, 2528.
- [26] H. Lu, P. J. Tonge, *Curr. Opin. Chem. Biol.* **2010**, *14*, 467.
- [27] a) A. Guardia, G. Gulten, R. Fernandez, J. Gómez, F. Wang, M. Convery, D. Blanco, M. Martínez, E. Pérez-Herrán, M. Alonso, F. Ortega, J. Rullás, D. Calvo, L. Mata, R. Young, J. C. Sacchettini, A. Mendoza-Losana, M. Remuñán, L. Ballell Pages, J. Castro-Pichel, *ChemMedChem* **2016**, *11*, 687; b) X. He, A. Alian, P. R. Ortiz de Montellano, *Bioorg. Med. Chem.* **2007**, *15*, 6649; c) X. He, A. Alian, R. Stroud, P. R. Ortiz de Montellano, *J. Med. Chem.* **2006**, *49*, 6308.
- [28] L. Encinas, H. O'Keefe, M. Neu, M. J. Remuñán, A. M. Patel, A. Guardia, C. P. Davie, N. Pérez-Macias, H. Yang, M. A. Convery, J. A. Messer, E. Pérez-Herrán, P. A. Centrella, D. Álvarez-Gómez, M. A. Clark, S. Huss, G. K. O'Donovan, F. Ortega-Muro, W. McDowell, P. Castañeda, C. C. Arico-Muendel, S. Pajk, J. Rullás, I. Angulo-Barturen, E. Álvarez-Ruiz, A. Mendoza-Losana, L. Ballell Pages, J. Castro-Pichel, G. Evindar, *J. Med. Chem.* **2014**, *57*, 1276.
- [29] a) M. Martínez-Hoyos, E. Perez-Herran, G. Gulten, L. Encinas, D. Álvarez-Gómez, E. Alvarez, S. Ferrer-Bazaga, A. García-Pérez, F. Ortega, I. Angulo-Barturen, J. Rullás-Trincado, D. Blanco Ruano, P. Torres, P. Castañeda,

- S. Huss, R. Fernández Menéndez, S. González del Valle, L. Ballell, D. Barros, S. Modha, N. Dhar, F. Signorino-Gelo, J. D. McKinney, J. F. García-Bustos, J. L. Lavandera, J. C. Sacchetti, M. S. Jimenez, N. Martín-Casabona, J. Castro-Pichel, A. Mendoza-Losana, *eBioMedicine* **2016**, *8*, 291; b) P. S. Shirude, P. Madhavapeddi, M. Naik, K. Murugan, V. Shinde, R. Nandishaiah, J. Bhat, A. Kumar, S. Hameed, G. Holdgate, G. Davies, H. McMiken, N. Hegde, A. Ambady, J. Venkatraman, M. Panda, B. Bhandodkar, V. K. Sambandamurthy, J. A. Read, *J. Med. Chem.* **2013**, *56*, 8533.
- [30] U. H. Manjunatha, S. P. S. Rao, R. R. Kondreddi, C. G. Noble, L. R. Camacho, B. H. Tan, S. H. Ng, P. S. Ng, N. L. Ma, S. B. Lakshminarayana, M. Herve, S. W. Barnes, W. Yu, K. Kuhen, F. Blasco, D. Beer, J. R. Walker, P. J. Tonge, R. Glynn, P. W. Smith, T. T. Diagana, *Sci. Transl. Med.* **2015**, *7*, 269ra263.
- [31] H. H. Soutter, P. Centrella, M. A. Clark, J. W. Cuozzo, C. E. Dumelin, M.-A. Guie, S. Habeshian, A. D. Keefe, K. M. Kennedy, E. A. Sigel, D. M. Troast, Y. Zhang, A. D. Ferguson, G. Davies, E. R. Stead, J. Breed, P. Madhavapeddi, J. A. Read *Proc. Natl. Acad. Sci. U. S. A.* **2016**, *113*, E7880.
- [32] P. Kamsri, C. Hanwarinroj, N. Phusi, T. Pornprom, K. Chayajarus, A. Punkvang, N. Suttipanta, P. Srimanote, K. Suttisintong, C. Songsiriritthigul, P. Saparpakorn, S. Hannongbua, S. Rattanabunyon, S. Seetaha, K. Choowongkamon, S. Sureram, P. Kittakoop, P. Hongmanee, P. Santanirand, Z. Chen, W. Zhu, R. A. Blood, Y. Takebayashi, P. Hinchliffe, A. J. Mulholland, J. Spencer, P. Pungpo, *J. Chem. Inf. Model.* **2020**, *60*, 226.
- [33] M. Sabbah, V. Mendes, R. G. Vistal, D. M. G. Dias, M. Záhorská, K. Mikušová, J. Korduláková, A. G. Coyne, T. L. Blundell, C. Abell, *J. Med. Chem.* **2020**, *63*, 4749.
- [34] C. Songsiriritthigul, C. Hanwarinroj, B. Pakamwong, P. Srimanote, N. Suttipanta, S. Sureram, K. Suttisintong, P. Kamsri, A. Punkvang, J. Spencer, P. Kittakoop, P. Pungpo, *Proteins* **2022**, *90*, 898.
- [35] S. K. Wahan, G. Bhargava, V. Chawla, P. A. Chawla, *Bioorg. Chem.* **2024**, *146*, 107250.
- [36] S. Davoodi, F. Daryaei, J. N. Iuliano, J. Tolentino Collado, Y. He, A. C. Pollard, A. A. Gil, J. M. Aramini, P. J. Tonge, *Biochemistry* **2023**, *62*, 1943.
- [37] a) R. Rawat, A. Whitty, P. J. Tonge, *Proc. Natl. Acad. Sci. U. S. A.* **2003**, *100*, 13881; b) T. J. Sullivan, J. J. Truglio, M. E. Boyne, P. Novichenok, X. Zhang, C. F. Stratton, H. J. Li, T. Kaur, A. Amin, F. Johnson, R. A. Slayden, C. Kisker, P. J. Tonge, *ACS Chem. Biol.* **2006**, *1*, 43; c) S. R. Luckner, N. Liu, C. W. am Ende, P. J. Tonge, C. Kisker, *J. Biol. Chem.* **2010**, *285*, 14330; d) H. J. Li, C. T. Lai, P. Pan, W. Yu, N. Liu, G. R. Bommineni, M. Garcia-Diaz, C. Simmerling, P. J. Tonge, *ACS Chem. Biol.* **2014**, *9*, 986; e) P. Pan, S. E. Knudson, G. R. Bommineni, H. J. Li, C. T. Lai, N. Liu, M. Garcia-Diaz, C. Simmerling, S. S. Patil, R. A. Slayden, P. J. Tonge, *ChemMedChem* **2014**, *9*, 776; f) C. T. Lai, H. J. Li, W. Yu, S. Shah, G. R. Bommineni, V. Perrone, M. Garcia-Diaz, P. J. Tonge, C. Simmerling, *Biochemistry* **2015**, *54*, 4683; g) L. A. Spagnuolo, S. Eltschkner, W. Yu, F. Daryaei, S. Davoodi, S. E. Knudson, E. K. Allen, J. Merino, A. Pschibul, B. Moree, N. Thivalapill, J. J. Truglio, J. Salafsky, R. A. Slayden, C. Kisker, P. J. Tonge, *J. Am. Chem. Soc.* **2017**, *139*, 3417.
- [38] a) E. M. Cohen, K. S. Machado, M. Cohen, O. N. de Souza, *BMC Genomics* **2011**, *12*, S7. b) R. S. Dasoondi, T. L. Blundell, A. P. Pandurangan, *Comput. Struct. Biotechnol. J.* **2023**, *21*, 1874; c) R. De Paris, C. V. Quevedo, D. D. Ruiz, O. Norberto de Souza, *PLoS One* **2015**, *10*, e0133172; d) R. De Paris, C. Vahl Quevedo, D. D. Ruiz, F. Gargano, O. N. de Souza, *BMC Bioinformatics* **2018**, *19*, 235; e) V. Kumar, M. E. Sobhia, *PLoS One* **2015**, *10*, e0144635; f) B. Merget, C. A. Sotriffer, *PLoS One* **2015**, *10*, e0127009; g) E. K. Schroeder, L. A. Basso, D. S. Santos, O. Norberto de Souza, *Biophys. J.* **2005**, *89*, 876; h) D. J. Shaw, K. Robb, B. V. Vetter, M. Tong, V. Molle, N. T. Hunt, P. A. Hoskisson, *Sci. Rep.* **2017**, *7*, 4714.
- [39] L. Maveyraud, L. Mourey, *Molecules* **2020**, *25*, 1030.
- [40] H. M. Berman, J. Westbrook, Z. Feng, G. Gilliland, T. N. Bhat, H. Weissig, I. N. Shindyalov, P. E. Bourne, *Nucleic Acids Res.* **2000**, *28*, 235.
- [41] E. Krissinel, K. Henrick, *Acta Crystallogr. Sect. D-Struct. Biol.* **2004**, *60*, 2256.
- [42] a) B. Lee, F. M. Richards, *J. Mol. Biol.* **1971**, *55*, 379-1N374; b) E. B. Saff, A. B. J. Kuijlaars, *Math. Intell.* **1997**, *19*, 5.
- [43] J. Agirre, M. Atanasova, H. Bagdonas, C. B. Ballard, A. Basle, J. Beilsten-Edmands, R. J. Borges, D. G. Brown, J. J. Burgos-Marmol, J. M. Berrisford, P. S. Bond, I. Caballero, L. Catapano, G. Chojnowski, A. G. Cook, K. D. Cowtan, T. I. Croll, J. E. Debreczeni, N. E. Devenish, E. J. Dodson, T. R. Drevon, P. Emsley, G. Evans, P. R. Evans, M. Fando, J. Foadi, L. Fuentes-Montero, E. F. Garman, M. Gerstel, R. J. Gildea, et al., *Acta Crystallogr. Sect. D-Biol. Crystallogr.* **2023**, *79*, 449.
- [44] P. Emsley, B. Lohkamp, W. G. Scott, K. Cowtan, *Acta Crystallogr. Sect. D-Biol. Crystallogr.* **2010**, *66*, 486.
- [45] R Core Team, R: A language and Environment for Statistical Computing, R Foundation for Statistical Computing, Vienna (Austria) **2022**.
- [46] Posit Team, RStudio: Integrated Development Environment for R, Posit Software, PBC, Boston, MA (USA) **2024**.
- [47] M. Bojanowski, R. Edwards, alluvial: R Package for Creating Alluvial Diagrams, R package version: 0.1-2 ed., Vienna (Austria) **2016**.

Manuscript received: January 29, 2025

Revised manuscript received: April 2, 2025

Version of record online: April 29, 2025